Semicircular Josephson junction embedded in a magnetic field

P. D. Shaju* and V. C. Kuriakose†
Department of Physics, Cochin University of Science and Technology, Cochin 682 022, India
(Received 19 December 2001; revised manuscript received 1 March 2002; published 22 May 2002)

A semicircular geometry is proposed for overlap Josephson junctions for experimental realization. Analytical and numerical studies on semicircular junctions show that an external static magnetic field applied parallel to the dielectric barrier interacts through the interior of the junction and produces a tilted potential which pushes out trapped fluxons from the interior of the junction, and a flux-free state exists in the junction in the absence of an external bias. Due to the semicircular shape, the effective field at the ends of the junction has opposite polarities which support penetration of opposite polarity fluxons into the junction in the presence of a forward-biased dc current. When the direction of the dc current is reversed, flux penetration is not possible and a flux-free state exists in the junction. Thus this geometry can be used in implementing a fluxon-based diode. The rectification properties of the junction are demonstrated using square-wave signals and sinusoidal ac signals. In the forward-biased state, fluxons and antifluxons enter the junction and move in opposite directions. Using this property, we propose and demonstrate a bidirectional flux-flow oscillator.

DOI: 10.1103/PhysRevB.65.214508 PACS number(s): 74.50.+r, 85.25.Cp, 05.45.Yv

I. INTRODUCTION

Fluxon dynamics in nonrectangular Josephson junctions (JJ's) has attracted much attention in recent years. The nonrectangular shape creates nonuniformity in the junction which can be advantageously employed in certain Josephson devices. In flux-flow oscillators, nonuniformity is used to reduce self-field effects and to facilitate unidirectional fluxon motion.[1] In Josephson trigger circuits, nonuniformity is employed to make a special dependance of the critical current upon the magnetic field.[2] Nonuniformity may mean unequal conditions for Josephson vortices in different parts of the junction. It may be due to the nonuniform spatial distribution of critical and bias currents,[3] temperature gradient effects,[4] nonuniform thicknesses of the dielectric barrier,[5] or to many other reasons.

Theoretical predictions on conventional JJ's such as overlap, in-line, and annular geometries under various internal and external conditions have been investigated and experimentally verified during the past years. Among the conventional geometries, annular geometry is widely used for experimental studies due to the fact that fluxons can be driven without any collision with the boundary.[6] Soliton dynamics in the presence of an open boundary complicates the analysis and interpretation of the experimental data. Recently, some complicated dynamics was predicted in single overlap junctions[7] and in a system of two and three JJ's coupled inductively[8,9] and at common end points.[10] Advances in lithography and low-temperature techniques have made possible the fabrication of highly complex tunnel junction-based structures, and investigations of fluxon dynamics in these unconventional structures, such as multistacked junctions (both linear[11] and annular[12]) and nonsymmetric and nonuniform junctions,[13] etc., are being carried out by a number of authors.

Progressive fluxon motion in a dissipative junction is supported by a dc driving force. The Lorentz force associated with the dc current drives the fluxons. However, it is shown that in the presence of a periodic spatial modulation, a low-frequency ac current can be effectively used to propagate the fluxons.[14] This is possible due to the resonant transfer of energy from the ac bias to the fluxon.[15] A microwave field irradiating JJ's gives rise to an ac drive[16] acting on the fluxon, which produces Shapiro steps in the absence of a dc current. This effect produces constant voltage steps crossing the zero-current axis.[17] A static magnetic field applied parallel to the barrier in a linear long overlap Josephson junction (LOJJ) has no effect in the interior part of the junction and the small perturbation produced is through the open boundary.[18,19] The effect of a spatially homogeneous static magnetic field on annular JJ's has undergone various theoretical and experimental studies.[20] The external field produces a periodic potential in the annular junction which can be used to trap the fluxons.[21]

In the present work, we investigate the effects of an external homogeneous static magnetic field on the propagation of fluxons in a dissipative LOJJ having a semicircular shape. Analytical and numerical studies show that the field interacts through the interior of the junction as well as through the boundary conditions and can exert a driving force supporting transitory motion (from one end to the other) for any trapped static flux quanta inside the junction. Thus under static conditions, a flux-free state exists in the junction. The main result of this work can be seen in the fact that opposite polarity fluxons can enter the junction from opposite ends and can move into the interior only if the junction is biased in one direction (forward bias). If the direction of the bias is reversed (reverse bias), fluxons cannot enter the junction due to the repulsive Lorentz force and the flux-free state that exists in the junction. Thus the junction exhibits the basic properties of a diode. By controlling the strength of the magnetic field, it is possible to get a single fluxon and a single antifluxon configuration in the junction. A detailed analysis shows that this single fluxon-antifluxon state ($\langle\uparrow\downarrow\rangle$) is highly stable against fluctuations. The stable dynamics exhibited by this fluxon-antifluxon pair is utilized in constructing the fluxon-based diode. It is found that even in the forward-biased state, there is a threshold value of the current

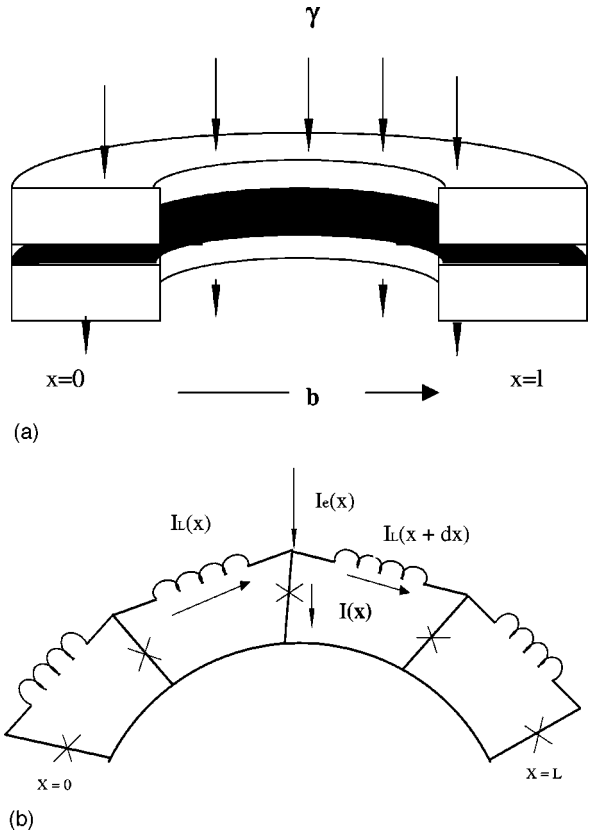

FIG. 1. Sketch of the SOJJ with the applied field *b*. (b) Schematic representation of the junction using discrete elements.

below which fluxons cannot enter into the junction. It is found that a small external magnetic field can damp the motion of a single trapped fluxon in the junction. In Sec. II, we introduce the semicircular overlap Josephson junction (SOJJ) and derive the perturbed sine-Gordon (SG) equation which is used in the numerical simulations. In Sec. III, we present the numerical methods and study the general properties of the junction, such as dc current-voltage characteristics (*IV*C), threshold values of the forward bias allowing fluxon propagation in the junction, and the damping effects of the magnetic field. In Sec. IV, we make use of the stable dynamics of the $\langle\uparrow\downarrow\rangle$ pair under a low magnetic field and demonstrate the rectification properties of the junction using a square wave and a sinusoidal ac current. The possibility of making a bidirectional flux-flow oscillator is discussed in Sec. V. In Sec. IV, we discuss the obtained results and present the conclusions.

II. THE THEORETICAL MODEL

An overlap JJ with a semicircular shape is considered [see Fig. 1(a)] with the discrete model shown in Fig. 1(b). An external static magnetic field applied parallel to the dielectric barrier interacts nonuniformly and produces a spatially varying perturbation. The Kirchhoff equations for the Josephson phases in the cell and for the currents in one of the nodes are

$$\varphi(X+dX)-\varphi(X)=\frac{2\pi}{\Phi_0}[d\Phi_e(X)-L^pI_L(X)], \tag{1}$$

$$I_L(X-dX)-I_L(X)=I(X)-I_e(X), \tag{2}$$

where $\varphi(X)$ is the Josephson phase at the point X of the junction, $d\Phi_e(X)$ is the component of the external magnetic flux linked with the cell of length dX, and L^p is the inductance of the piece of the junction electrodes between X and $X+dX$. $I_L(X)$ is the current through the inductance, $I_e(X)$ is the externally applied current, $I(X)$ is the current through the Josephson junction, and $\Phi_0=h/2e=2.064\times10^{-15}$ Wb is the flux quantum.

The external magnetic field $\hat{B}$ interacts with the interior of the junction and the component of the external flux in the plane of the junction over an infinitesimal interval dX is calculated as[15,20–22]

$$d\Phi_e(X)=\Delta(\hat{B}\cdot\hat{n})dX=\Delta B\cos(KX)dX, \tag{3}$$

where Δ is the coupling of the external magnetic field with the junction, and $\hat{n}$ is the unit vector normal to the propagation direction and in the plane of the junction. Thus a homogeneous static field makes an effective nonhomogeneous field inside the junction. From Eq. (3), it is clear that for a linear junction (i.e., if $\hat{n}$ is independent of X) in a homogeneous magnetic field there will be no perturbation from the magnetic field to the interior of the junction. In this case there would only be interaction through the open boundary conditions. However, if the junction has a semicircular shape or any other curved shape, $\hat{n}$ depends on X and there is perturbation to the interior of the junction.

Using the relations

$$L^p=L'dX,\ \ I(X)=j(X)dX,\ \ I_e(X)=-j_e(X)dX \tag{4}$$

and substituting Eq. (3) into Eqs. (1) and (2), we write the latter in the following form:

$$\frac{\partial I_L(X)}{\partial X}=-\frac{\Phi_0}{2\pi L'}\frac{\partial^2\varphi}{\partial X^2}-\frac{\Delta BK}{L'}\sin(KX), \tag{5}$$

$$\frac{\partial I_L(X)}{\partial X}=-j_e(X)-j(X), \tag{6}$$

where L' is the inductance per unit length of the junction, $K=\pi/L$ is the spatial periodicity of the field inside the junction, and L is the length of the junction. We assume that the dielectric is spatially uniform so that Δ and L' are independent of X. In the case of a simple resistively shunted junction model, the supercurrent density $j(X)$ is the sum of the supercurrent, normal (quasiparticle) current, and displacement current densities,

$$j(X)=j_0\sin\varphi+\frac{\Phi_0}{2\pi R}\varphi_T+\frac{C\Phi_0}{2\pi}\varphi_{TT}. \tag{7}$$

Here j_0, R, and C are the critical current density, specific resistance, and specific capacitance of the junction, respectively. Using Eqs. (5)–(7) we get the SG equation

$$\frac{C\Phi_0}{2\pi}\varphi_{TT}-\frac{\Phi_0}{2\pi L'}\frac{\partial^2\varphi}{\partial X^2}+j_0\sin\varphi$$

$$=-\frac{\Phi_0}{2\pi R}\varphi_T+\frac{\Delta BK}{L'}\sin(KX)-j_e(X). \tag{8}$$

The component of the external flux over an infinitesimal distance dX of the unit cell in terms of the quantized unit is

$$d\varphi(X)=\frac{2\pi}{\Phi_0}d\Phi_e(X)=\frac{2\pi}{\Phi_0}\Delta B\cos(KX)dX. \tag{9}$$

The effect of an applied magnetic field on the junction is to induce currents in closed form across the junction. So the net current when integrated over the junction should be zero. Due to the semicircular shape, the external field induces a varying surface current along the junction. Since the spatial derivative of the superconducting phase is equivalent to the induced surface current, we get

$$\frac{d\varphi(X)}{dX}=\frac{2\pi}{\Phi_0}\Delta B\cos(KX). \tag{10}$$

This equation can be used to obtain the boundary conditions of the junction. Using the normalized quantities, $T=t/\omega_0$, $X=x\lambda_J$, $\lambda_J=(\Phi_0/2\pi L\, j_0)^{1/2}$, and $\omega_0=(2\pi j_0/C\Phi_0)^{1/2}$ in Eq. (8) we get the general perturbed SG partial differential equation

$$\varphi_{tt}-\varphi_{xx}+\sin\varphi=-\alpha\varphi_t+b\,\sin(kx)-\gamma, \tag{11}$$

where $\varphi(x,t)$ is the superconducting phase difference between the electrodes of the junction, the spatial coordinate x is normalized to λ_J, the time t is normalized to the inverse plasma frequency ω_0, the dissipative parameter $\alpha=1/CR\omega_0$ takes into account the tunneling of normal electrons across the junction, γ is the dc bias current normalized to the Josephson critical current density j_0, $k=\pi/l$, and $b=2\pi\lambda_j\Delta Bk/\Phi_0=2\,k(B/B_{c1})$, where $B_{c1}=\Phi_0/\pi\Delta\lambda_j$ is the first critical field of the Josephson junction.

Compared with the standard sine-Gordon model for Josephson junctions, this equation has an extra term $b\sin(kx)$, which corresponds to a force that drives fluxons towards the left and antifluxons towards the right. Therefore any static trapped fluxon present in the junction will be removed and a flux-free state will exist in the junction in the absence of an external bias. Thus the effect of the external field is to act like a bias current $\gamma_b=b\sin(kx)$, which has a nonzero average in space. This bias current stops penetration of fluxons from the left end and penetration of antifluxons from the right end. So the junction does not support any fluxons in the static conditions. This nonzero average current (see Fig. 2) induces a nonperiodic field (potential) inside the junction.

From Eq. (10), we get the corresponding boundary conditions of the junction to be

$$\varphi_x(0,t)=\frac{b}{k},$$

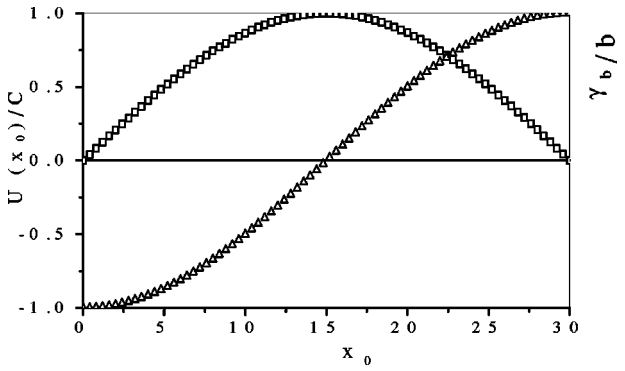

FIG. 2. Tilted potential $U(x_0)/C$ along the junction as a function of the fluxon coordinate x_0 (triangles) and the field-induced bias term γ_b/b (squares) for a junction of $l=30$.

$$\varphi_x(l,t)=-\frac{b}{k}. \tag{12}$$

These boundary conditions are consistent with the fact that effective field linked with the junction has opposite polarities at the ends of the junction. So only fluxons can enter from the left end ($x=0$) and antifluxons from the right end ($x=l$) in a properly biased junction. From Eq. (11), we see that fluxons can enter from the left end and antifluxons can enter from the right end of the junction for positive values of γ (forward-biased state). Negative values of γ drive fluxons towards the left and antifluxons towards the right and fluxon penetration becomes impossible (reverse-biased state). Equation (11) with a boundary condition [Eq. (12)] represents a SOJJ in a homogeneous static magnetic field. In the absence of perturbations ($\alpha=\gamma=b=0$), Eq. (11) becomes the SG equation which is a conservative, nonlinear dispersive wave equation that supports special solutions called solitons. A SG soliton is a localized wave that is analytically described by the formula[23]

$$\varphi(x,t)=4\tan^{-1}\left[\exp\frac{\sigma(x-x_0)}{\sqrt{1-u^2}}\right], \tag{13}$$

where $x_0=ut+x_0'$ is the location of the soliton with u as the velocity of the soliton and x_0' as the initial location center. $\sigma=\pm1$ is the polarity of the flux quantum. The LOJJ could support the resonant propagation of fluxons trapped in the junction, if the soliton is a 2π jump in the phase difference φ across the insulating barrier which separates the two superconductors. There are two possible orientations for the flux. A quantum of flux in one direction is called a kink soliton (fluxon) and that in the opposite direction is called an antikink soliton (antifluxon). The moving soliton is accompanied by a voltage pulse φ_t which can be detected across the junction.

The Lagrangian density of Eq. (11) with $\alpha=\gamma=0$ is

$$\mathbf{L}=\left\{\frac{\varphi_t^2}{2}-\frac{1}{2}\left(\varphi_x-\frac{b}{k}\cos(kx)\right)^2-(1-\cos\varphi)\right\}. \tag{14}$$

Therefore the corresponding potential-energy density is (second term in the above equation)

$$\mathbf{U}(x)=\frac{1}{2}\left\{\varphi_x^2-\frac{2b}{k}\cos(kx)\varphi_x+\left(\frac{b}{k}\cos(kx)\right)^2\right\}. \quad (15)$$

The first term is independent of the applied field and the third term is a constant which is independent of the flux motion in the junction. Therefore the change in the potential due to the applied field can be determined from the second term to be

$$U(x)=-\frac{b}{k}\int_{-\infty}^{+\infty}\varphi_x\cos(kx)dx. \quad (16)$$

Substituting Eqs. (13) in (16) and integrating, we get

$$U(x_0)=-2bl\,\mathrm{sec}\,h\left(\frac{\pi^2}{2l}\sqrt{1-u^2}\right)\cos(kx_0). \quad (17)$$

For long junctions and those at relativistic velocities, $u\sim 1$, Eq. (17) becomes

$$U(x_0)=-C\cos(kx_0), \quad (18)$$

where $C=2\,bl$ is a constant. Equation (18) shows that the potential is tilted by the applied field (see Fig. 2). Tilting is either to the left or the right side of the junction depending on the direction of the field. This tilt in the potential causes trapped static fluxons and antifluxons to move in opposite directions and thus the junction remains flux-free under static conditions. Thus any trapped flux can be removed from the junction by applying a static magnetic field.

Energy of the unperturbed SG system is

$$H^{SG}=\int_0^l\left[\frac{1}{2}(\varphi_t^2+\varphi_x^2)+1-\cos\varphi\right]dx. \quad (19)$$

Perturbational parameters modulate the velocity of the solitons and may cause the energy to dissipate. The rate of dissipation is calculated by computing

$$\frac{d}{dt}(H^P)=[\varphi_x\varphi_t]_0^l+\int_0^l \times\{-\alpha\varphi_t^2+[b\sin(kx)-\gamma]\varphi_t\}dx, \quad (20)$$

where the first term on the right side accounts for the boundary conditions. From Eq. (13) we get $\varphi_t=-u\varphi_x$ and from Eq. (12), $\varphi_x^2(0,t)=\varphi_x^2(l,t)$ (symmetric boundary conditions). Substituting these expressions, we find that the first term on the right-hand side of the above equation vanishes—a symmetric boundary condition does not change the average energy value of a fluxon. Inserting Eq. (13) into Eqs. (19) and (20), and following a perturbative analysis,[23] we get

$$(1-u^2)^{-3/2}\frac{du}{dt}=-\alpha\frac{u}{\sqrt{1-u^2}} -\frac{\pi}{4}\left\{b\,\mathrm{sec}\,h\left[\frac{\pi^2\sqrt{1-u^2}}{2l}\right]\sin(kx_0)-\gamma\right\}. \quad (21)$$

This expression describes the effect of perturbations on the fluxon velocity. In the absence of dc bias (i.e., $\gamma=0$), from Eq. (21) we get for the threshold value of the magnetic field for producing equilibrium velocity (i.e., at $du/dt=0$) on a trapped fluxon

$$b=-\frac{4\alpha}{\pi}\frac{u_0}{\sqrt{1-u_0^2}}\frac{1}{\mathrm{sec}\,h\left[\frac{\pi^2\sqrt{1-u_0^2}}{2l}\right]\sin(kx_0)}. \quad (22)$$

For long junctions, $\pi^2/2l\ll 1$, we obtain for the approximate equilibrium velocity of the fluxon when $u_0\sim 1$ with $x_0'=l/2$

$$u_0\simeq\pm\left[1+\left(\frac{4\alpha}{\pi b}\right)^2\right]^{-1/2}. \quad (23)$$

This equilibrium velocity is equivalent to that obtained in Ref. 23 with a dc bias. Thus it can be concluded that in SOJJ, the magnetic field exerts a driving force on trapped fluxons and produces a transitory motion in the junction.

The effects of a dc current on the fluxon dynamics in the presence of the external field are studied using Eq. (11). Even in the forward-biased state, a zero-voltage state (ZVS) exists in the junction (flux-free state) when the driving force due to the field (γ_b) and to the dc current (γ) is nearly equal and in opposite directions. By variation of the soliton position x_0', from Eq. (21), we find the largest possible bias current of the ZVS ($u=0$) to be[20]

$$\gamma_1=b\,\mathrm{sec}\,h\left(\frac{\pi^2}{2l}\right). \quad (24)$$

This is the threshold value of the applied bias, below which flux propagation is not possible in the junction. This threshold value depends on the magnetic field and is directly proportional to the field.

III. NUMERICAL RESULTS

To solve Eqs. (11) and (12), we use an explicit method to treat φ_{xx} with a five-point, φ_{tt} with a three-point, and φ_t with a two-point symmetric finite-difference method. The boundary conditions are treated by the introduction of imaginary points [i.e., $\varphi(-x,t)=\varphi(x,t)$]. The nonlinear term is evaluated using a predictor-corrector loop. A time step of 0.0125 and a space step of 0.025 are used for the discretization. Calculations are rechecked by systematically halving and doubling the time and space steps. Details of the simulation can be found in Refs. 7–9. After the simulation of the phase dynamics for a transient time, we calculate the average voltage V for a time interval T to be

$$V=\frac{1}{T}\int_0^T\varphi_t dt=\frac{\varphi(T)-\varphi(0)}{T}. \quad (25)$$

For faster convergence of our averaging procedure, we additionally averaged the phases $\varphi(x)$ in Eq. (25) over the length of the junction. Once the voltage averaging for a current γ is complete, the current γ is increased by a small amount $\delta\gamma=0.01$ to calculate the voltage at the next point of the IVC. We use a distribution of the phases and their derivatives achieved in the previous point of the IVC as the initial distribution for the following point. The average velocity of the

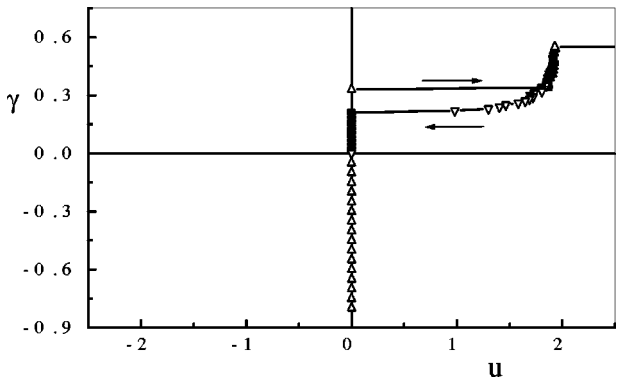

FIG. 3. Applied dc bias γ versus the average velocity $u = V(l/2\pi)$ in the junction in the forward-biased state and in reverse-biased state. Arrows indicate the direction of the sweeping current. Other parameters are $l=34$, $\alpha=0.1$, and $b=0.1$.

fluxons can be calculated from the average voltage using the relation $u=V(l/2\pi)$. Thus the mean voltage in the junction is proportional to the average velocity of the fluxons. The instantaneous voltage pulse form across the junction is calculated using

$$V(t)=\frac{1}{l}\int_0^l \varphi_t dx, \tag{26}$$

where we have averaged the voltage pulses over the length of the junction.

A. Properties of the junction under a dc bias

Figure 3 shows the average velocity (equivalently average voltage) attained by the fluxon-antifluxon pair $\langle\uparrow\downarrow\rangle$ as a function of the dc bias in the junction in the forward-biased (positive values of γ) state and in the reverse-biased state (negative values of γ). We have considered a junction of length $l=34$ and dissipation parameter $\alpha=0.1$. The field strength is fixed at $b=0.1$. The system is started with $\varphi=0$ and $\partial\varphi/\partial t=0$. For positive values of the sweeping dc current, flux penetration is possible in the junction. A ZVS corresponding to the flux-free state exists in the junction up to a bias value of $\gamma=0.32$. At this threshold value, a fluxon enters the junction from the left end and an antifluxon from the right end simultaneously and they move in opposite directions in the junction under the influence of the dc bias. This fluxon-antifluxon pair is found to be stable for sufficiently larger bias values. The dynamics of the pair $\langle\uparrow\downarrow\rangle$ in the junction gives an average normalized maximum velocity of $u=2$. This pair executes a highly stable motion up to a bias value of $\gamma=0.58$. On increasing the bias values further, a large number of fluxons and antifluxons enter into the junction and they make successive reflections at the boundaries which results in a switching of the *IV*C to high-voltage states. We have not pursued the high-voltage states of the junction since the number of fluxons taking part in the dynamics is not fixed. In the reverse sweep of the bias, i.e., on decreasing the bias uniformly in very small steps, we observed hysteresis in the dynamics and finite voltage is observed up to $\gamma=0.22$. In Fig. 4, the spatial derivative of the

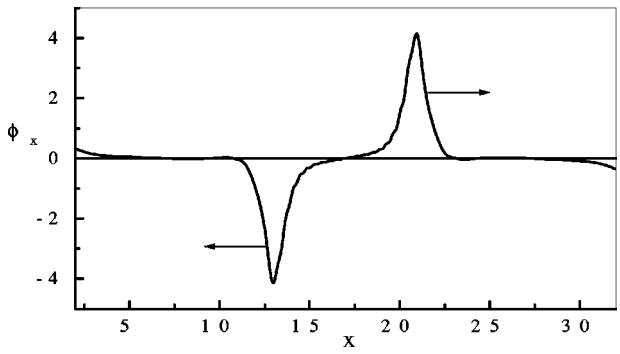

FIG. 4. Spatial profile (φ_x) of the fluxon-antifluxon pair $\langle\uparrow\downarrow\rangle$ in the junction corresponding to the dynamics in Fig. 3.

phase (φ_x) in the state $\langle\uparrow\downarrow\rangle$ along the junction is plotted. A fluxon on entering from the left end moves towards the right end and an antifluxon on entering from the right end moves towards the left end. For negative values of the dc bias, flux penetration is not possible and a ZVS (flux-free state) exists for all values of the negative dc bias. In this region the junction behaves as a reverse-biased diode.

The threshold values of the dc bias (γ_1) allowing propagation of a single fluxon in the junction at various values of the field are shown in Fig. 5. The threshold value increases on increasing the magnetic field. To determine the threshold values, we have considered the dynamics of a single trapped fluxon in the junction. Below the threshold value propagation is not possible in the junction and the trapped fluxon is annihilated. A small magnetic field applied to the junction can damp the motion of a trapped fluxon. On increasing the field, the fluxon slows down and is finally annihilated in the junction. In Fig. 6, the damping effects of a small field are shown for a trapped fluxon moving under different values of the dc bias.

IV. ac BIAS—DEMONSTRATION OF A FLUXON DIODE

A detailed analysis shows that the SOJJ embedded with the static magnetic field has the characteristics of a diode. Thus fluxon-based diodes can be implemented using this ge-

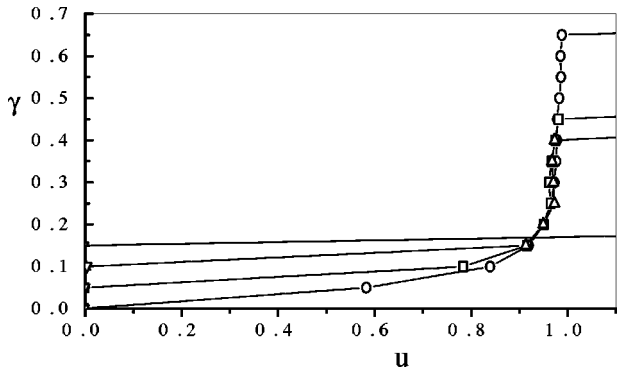

FIG. 5. IVC of a single trapped fluxon in the junction showing the threshold value of the bias current (γ_1) for different magnetic-field values. ZVS exists below the threshold value γ_1. Parameters are $l=20$, $\alpha=0.05$, $b=0.0$ (circles), $b=0.1$ (squares), $b=0.12$ (up triangles), and $b=0.15$ (down triangles).

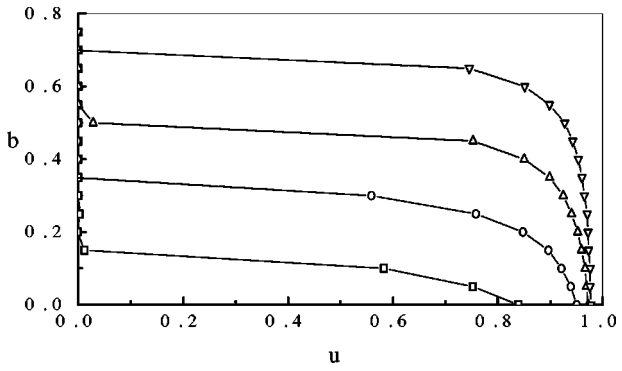

FIG. 6. Damping effects of the magnetic field on the velocity of a single trapped fluxon in the junction. Parameters are $l=20$, $\alpha=0.05$, $\gamma=0.10$ (squares), $\gamma=0.2$ (circles), $\gamma=0.3$ (up triangles), and $\gamma=0.4$ (down triangles).

ometry. To demonstrate the rectification effects, we use the pair $\langle\uparrow\downarrow\rangle$ dynamics in the junction. The *IV*C of the SOJJ shows that fluxons and antifluxons can enter the junction only if the junction is forward biased and fluxon dynamics is not possible in the reverse-biased state. Figure 7 demonstrates the forward-biased state and reverse-biased state of the junction. In the forward-biased state [positive values of γ in Eq. (11)], the pair $\langle\uparrow\downarrow\rangle$ is highly stable against perturbations. This pair exists for sufficiently higher values of the dc bias. In the reverse-biased state (negative values of γ), fluxons cannot exist in the junction and the ZVS exists for all values of the negative bias. We have considered different parameters of the junction and found that the pair executes symmetric motion in the junction under the influence of the dc bias.

A. Rectification of a square wave

To demonstrate rectification effects of an ac current we used a square wave

$$\gamma=-\begin{cases} A & 0\leqslant t<T/2 \\ -A & T/2\leqslant t<T \end{cases}$$

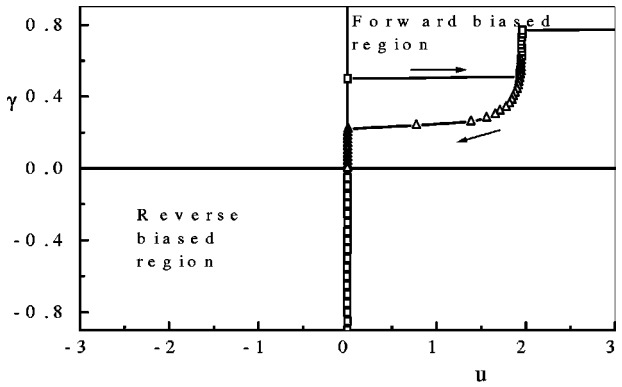

FIG. 7. Forward- and reverse-biased states of a fluxon diode. Applied dc bias γ versus the average velocity u of a fluxon-antifluxon pair in the junction in the forward-biased state and the reverse-biased state. Zero voltage exists in the reverse-biased state. Arrows indicate the directions of the sweeping current. Other parameters are $l=20$, $\alpha=0.1$, and $b=0.12$.

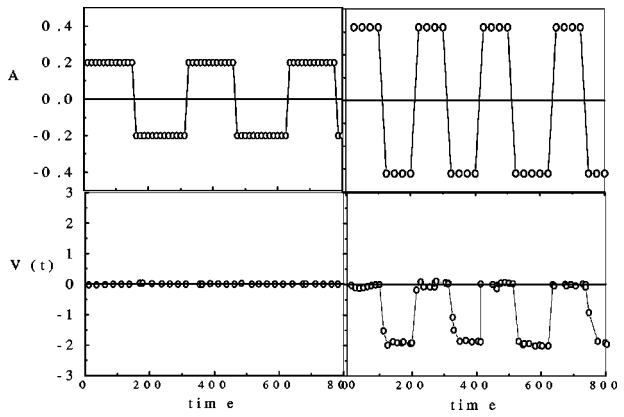

FIG. 8. Rectification of a square wave. Left panel shows zero output voltage for the input amplitude $A=0.20$. Right panel shows rectified voltage pulses for input amplitude $A=0.32$. Frequency of the signal is $\omega=0.02$. Other parameters are $l=34$, $\alpha=0.1$, and $b=0.11$.

in Eq. (11). The period of the square wave is taken to be much larger than the typical response time of the system (~ 1 ns) so that it is in the adiabatic regime. The amplitude of the ac signal should be sufficiently large to induce flux motion in the junction. In the first half cycle of the square wave, fluxon penetration is not possible and zero voltage exists in the junction. In the second half cycle, one fluxon enters from the left end and one antifluxon from the right end and the pair $\langle\uparrow\downarrow\rangle$ moves in opposite directions. The strength of the external field is adjusted in such a way that no more fluxons can enter into the junction. The rectification process is demonstrated in the time domain snapshots of Fig. 8, where we plot the instantaneous voltage $[V(t)]$ across the junction as a function of time. If the amplitude of the ac signal is below a threshold value, the ZVS exists in the junction as can be seen in the left panel of Fig. 8. In Fig. 9, we plot the average voltage (averaged over a period of the input signal) as a function of the amplitude of the square wave. The average voltage increases on increasing the amplitude of the input signal. The ZVS exists if the amplitude is below 0.56 (peak to peak, $A=0.26$) and the output voltage in-

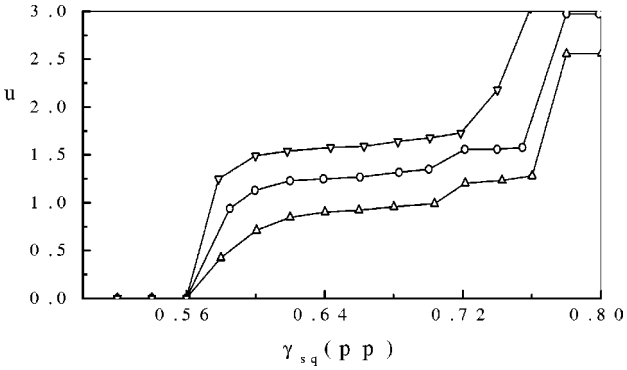

FIG. 9. Square-wave amplitude versus average velocity in the junction for different values of the input signal frequency. Parameters are $l=34$, $\alpha=0.1$, $b=0.10$,$A=0.32$, $\omega=0.02$ (down triangles), $\omega=0.03$ (circles), and $\omega=0.04$ (up triangles).

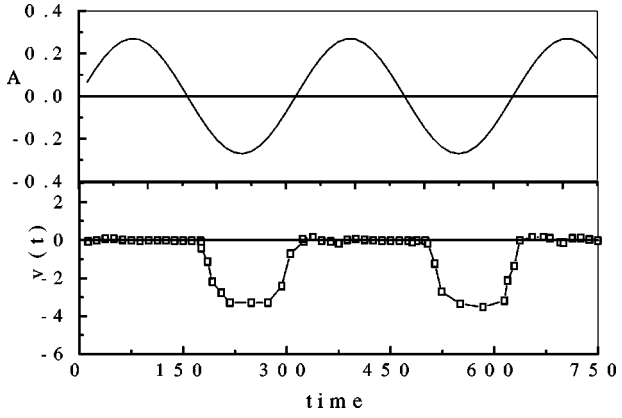

FIG. 10. Voltage pulses $[V(t)]$ across the junction as a function of time demonstrating rectification of a sine wave. Input signal of amplitude $A=0.27$ and frequency $\omega=0.02$ is used on a junction of length $l=25$ and $\alpha=0.1$. The applied field strength is fixed at $b=0.21$.

creases linearly in the range 0.6–0.7 of the square-wave amplitude. At higher values, additional fluxons enter into the junction so that the output is no longer proportional to the input current. We have considered different frequencies of the input signal and found that the pair $\langle\uparrow\downarrow\rangle$ gives stable and reliable results.

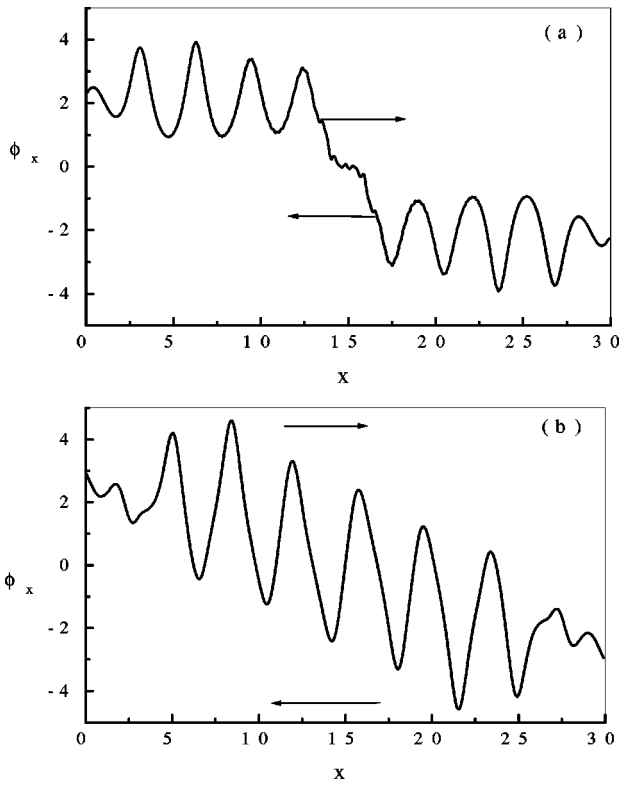

FIG. 11. (a) Spatial profile (φ_x) showing a train of fluxons entering the junction from the left end and a train of antifluxons entering from the right end in a junction of length $l=30$. (b) Spatial profile showing resonant propagation of fluxons towards the right end and antifluxons towards the left end.

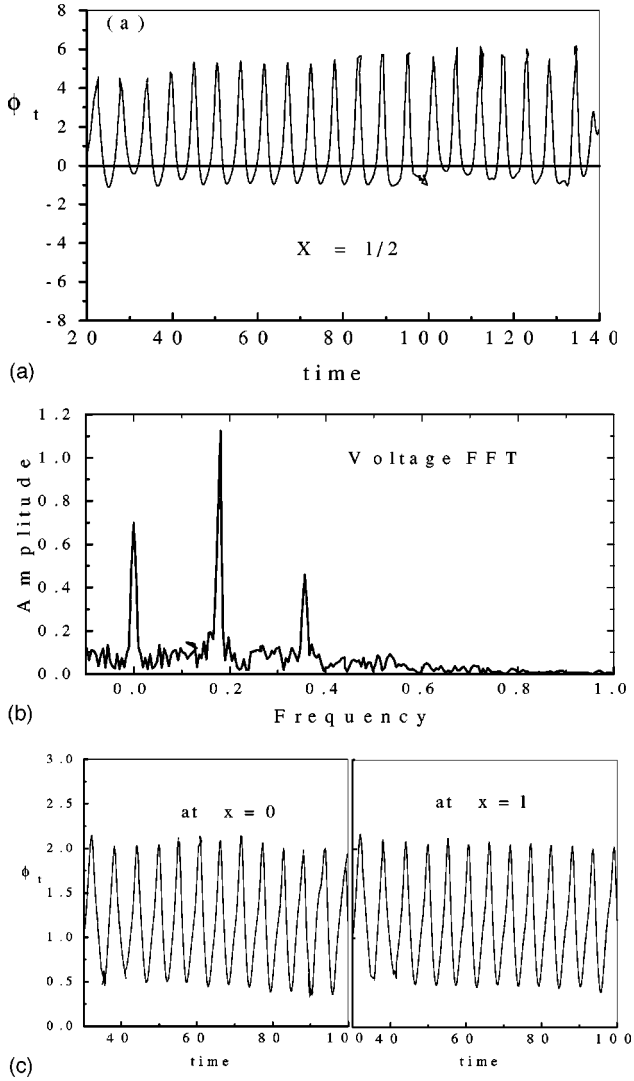

FIG. 12. Voltage pulses in the middle of the junction. Parameters are $l=20$, $\alpha=0.1$, $b=0.4$, $\gamma=0.4$, and $z=1.0$. (b) Fourier power spectrum of the voltage pulses measured in the middle ($x=l/2$) of the junction. Parameters are the same as in (a). Spectrum has been computed from 4250 data points. (c) Voltage pulses at the ends ($x=0$ and $x=l$) of the junction.

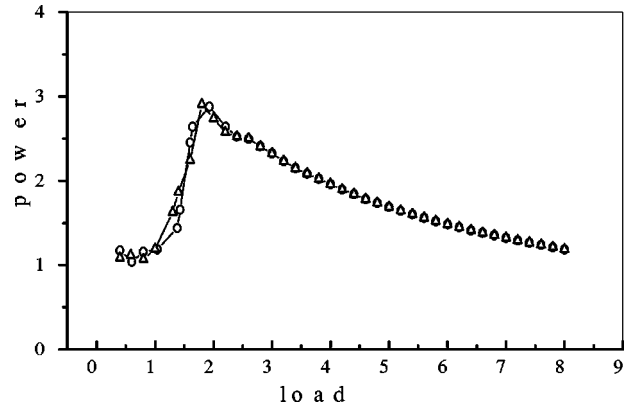

FIG. 13. Average output power versus load z on the left end of the junction (circles) and the right end of the junction (triangles). Parameters are the same as in Fig. 12(a).

B. Rectification of a sine wave

To study the rectification properties of sinusoidal ac currents, we used a sine wave $\gamma = -A\sin(\omega t)$ in Eq. (11). The period of the signal is taken to be much higher than the typical response time of the system. The frequency of the signal used is $\omega = 0.02$. The dynamics of the pair $\langle\uparrow\downarrow\rangle$ is studied under a magnetic field of strength $b = 0.21$ on a junction of length $l = 25$ and dissipation parameter $\alpha = 0.1$. Figure 10 shows the time domain voltage pulses in the junction. We have considered different amplitudes and frequencies of the input signal and could achieve best results using the pair $\langle\uparrow\downarrow\rangle$.

V. FLUX-FLOW STATE—DEMONSTRATION OF A BIDIRECTIONAL FLUX-FLOW OSCILLATOR

To study the feasibility of making this device a flux-flow oscillator, we have done a preliminary study and investigated the flux dynamics of a group of fluxons under a large magnetic field. In the proposed oscillator, fluxons enter the junction from the left end and move towards the right end due to the applied bias (in the forward-biased state) and on reaching the right end, they are selectively terminated (a passive load of impedance z in a series with a diode is connected at the ends of the junction). In a similar way, antifluxons enter the junction from the right end and move towards the left end where they are terminated. In implementing the device, we used a special technique by which fluxons are absorbed selectively at the right end of the junction and antifluxons are absorbed at the left end of the junction. In experiment, this can be realized by using a load resistor in a series with a diode. At the right end, the diode should be placed in such a way that it allows the screening currents associated with the fluxons to go through the load (termination of fluxons) and disallows the screening currents associated with the antifluxons. Similarly at the left end, the diode should allow the screening currents of the antifluxons to go through the load (termination of antifluxons). Thus selective absorption of the fluxons can be achieved at the ends. Figure 11(a) shows the snapshots of the spatial profile (φ_x) of a group of fluxons entering from left end and antifluxons from the right end in the junction. Figure 11(b) shows the snapshots (φ_x) of the resonant motion of fluxons and antifluxons in the opposite directions in a coherent state. This resonant motion is highly stable and can be a mechanism for constructing the bidirectional oscillators. This resonant, coherent motion also helps to avoid any stray fluxons in the junction thus making the junction a highly tunable device. Figure 12(a) shows the corresponding time dependence of the voltage pulse form in the middle of the junction. All the voltage pulses are equally spaced showing spatial coherence in the junction. The calculated frequency spectrum (fast Fourier transform) of the voltage pulses is shown in Fig. 12(b). The figure shows the dominant first harmonic of the oscillations at frequency $f = 0.181$ (in normalized units) and the second harmonic at frequency $f = 0.362$. Figure 12(c) shows the time dependence of the voltage pulses on both ends of the junction. The pulses are symmetric and equally spaced which is a manifestation of the coherent motion of fluxons in the junction.

It is important for practical applications to know the influence of the load (z) on the average output power of the device, in particular, to see how it behaves for larger loads. Figure 13 shows the dependency of the average output power ($P = VI \equiv \varphi_t^2/z$) obtained from both ends as a function of the load for the values of the junction $l = 20$, $\alpha = 0.1$, $\gamma = 0.4$, and $b = 0.4$. The output power increases and maximizes at the impedance-matching condition and then decreases slightly on increasing the load. At larger values of the load the output become practically independent of the load, which is a desirable feature for using these devices as oscillators.

The main characteristics of this flux-flow oscillator is that both fluxons and antifluxons take part in the dynamics and because of that output can be obtained from both ends. Only in the resonant state can we get output from the junction and can the resonant state avoid any stray fluxons inside the junction. The oscillator can be tuned by tuning the dissipative junction parameters, applied dc bias currents, and the external magnetic-field values.

VI. CONCLUSION

In conclusion, we have studied flux-quantum dynamics in a semicircular geometry and the results suggest that this geometry can be used for fabrication of fluxon-based diodes for rectification of ac signals and for implementing bidirectional flux-flow oscillators. This particular geometry is easy to fabricate because of the symmetrical shape, and the main advantage is that opposite polarity fluxons can enter the junction simultaneously under a constant forward bias. Fluxons cannot enter the junction in the reverse-biased state. Using this property, fluxon-based diodes can be constructed. The magnetic-field-driven transit of a trapped flux quantum under static conditions can find applications in digital transmission lines and in flux cleaning in stacked junctions. In the forward-biased state, opposite polarity fluxons can enter the junction from the ends and can move in opposite directions. Using this property of the junction, bidirectional flux-flow oscillators can be implemented and the advantage is that we can get output from both ends of the junction. Using vertically stacked junctions, the power associated with the flux-flow oscillator can be increased considerably.

ACKNOWLEDGMENTS

One of the authors (P.D.S.) wishes to thank UGC, New Delhi, for financial support in the form of a teacher fellowship and V.C.K. wishes to acknowledge the Associateship of IUCAA, Pune.

*Email address: pds@cusat.ac.in
†Email address: vck@cusat.ac.in

[1] J.H. Thompson, M.A. Ketkar, J.B. Beyer, and J.E. Nordman, IEEE Trans. Appl. Supercond. **3**, 2543 (1993).
[2] S.A. Vasenko, K.K. Likharev, and V.K. Semenov, Zh. Eksp. Teor. Phys. **4**, 1444 (1981) [Sov. Phys. JETP **54**, 766 (1981)].
[3] A. Barone and G. Paternó, *Physics and Applications of the Josephson Effect* (Wiley, New York, 1982).
[4] V.M. Krasnov, V.A. Oboznov, and N.F. Pedersen, Phys. Rev. B **55**, 14 486 (1997).
[5] A. Benabdallah, J.G. Caputo, and N. Flytzanis, cond-mat/0106063 (unpublished).
[6] A. Davidson, B. Dueholm, B. Kryger, and N.F. Pedersen, Phys. Rev. Lett. **55**, 2059 (1985); A.V. Ustinov, T. Doderer, R.P. Huebener, N.F. Pedersen, B. Mayer, and V.A. Oboznov, *ibid.* **69**, 1815 (1992).
[7] P.D. Shaju and V.C. Kuriakose, Mod. Phys. Lett. B **12**, 1217 (1998).
[8] P.D. Shaju and V.C. Kuriakose, Physica C **322**, 163 (1999).
[9] P.D. Shaju and V.C. Kuriakose, Phys. Lett. A **267**, 420 (2000).
[10] S.A. Hattel, A. Grunnet-Jepsen, and M.R. Samuelsen, Phys. Lett. A **221**, 115 (1996); A. Grunnet-Jepsen, F.N. Fahrendorf, S.A. Hattel, N. Grønbech-Jensen, and M.R. Samuelsen, *ibid.* **175**, 116 (1993).
[11] S. Sakai, A.V. Ustinov, H. Kohlstedt, A. Petraglia, and N.F. Pedersen, Phys. Rev. B **50**, 12 905 (1994); A.V. Ustinov *et al.*, *ibid.* **48**, 10 614 (1993).
[12] E. Goldobin, A. Wallraff, N. Thyssen, and A.V. Ustinov, Phys. Rev. B **57**, 130 (1998).
[13] E. Goldobin, A. Sterck, and D. Koelle, Phys. Rev. E **63**, 031111 (2001); S. Pagano *et al.*, in *Nonlinear Superconducting Devices and High-*T_c *Materials*, edited by R. D. Parmentier and N. F. Pedersen (World Scientific, Singapore, 1995).
[14] G. Filatrella, B.A. Malomed, and R.D. Parmentier, Phys. Lett. A **198**, 43 (1995).
[15] A.V. Ustinov and B.A. Malomed, Phys. Rev. B **64**, 020302 (2001).
[16] M. Salerno, M.R. Samuelsen, G. Filatrella, S. Pagano, and R.D. Parmentier, Phys. Rev. B **41**, 6641 (1990).
[17] S. Shapiro, Phys. Rev. Lett. **11**, 80 (1963); Y.J. Doh, Jinhee Kim, K.T. Kim, and H.J. Lee, Phys. Rev. B **61**, R3834 (2000).
[18] M.P. Soerensen, N. Arley, P.L. Christiansen, R.D. Parmentier, and O. Skovgaard, Phys. Rev. Lett. **51**, 1919 (1983); W.J. Yeh, O.G. Symko, and D.J. Zheng, Phys. Rev. B **42**, 4080 (1990).
[19] B. Dueholm, E. Joergensen, O.A. Levring, J. Mygin, N.F. Pedersen, M.R. Samuelsen, O.H. Olsen, and M. Cirillo, Physica B & C **108B**, 1303 (1981); Yeh, Symko, and Zheng (Ref. 18).
[20] N. Grønbech-Jensen, P.S. Lomdahl, and M.R. Samuelsen, Phys. Lett. A **154**, 14 (1991).
[21] A.V. Ustinov, B.A. Malomed, and N. Thyssen, Phys. Lett. A **233**, 239 (1997).
[22] N. Grønbech-Jensen, P.S. Lomdahl, and M.R. Samuelsen, Phys. Rev. B **43**, 12 799 (1991); J.C. Fernandez, R. Grauer, K. Pinnow, and G. Reinisch, Phys. Lett. A **145**, 333 (1990); A. Wallraff *et al.*, J. Low Temp. Phys. **118**, 543 (2000).
[23] D.W. McLaughlin and A.C. Scott, Phys. Rev. A **18**, 1652 (1978).